Weakly Nonlinear Model with Exact Coefficients for the Fluttering and Spiraling Motion of Buoyancy-Driven Bodies

Joël Tchoufag,[1] David Fabre,[1] and Jacques Magnaudet[1,2,*]
[1]Université de Toulouse, Institut de Mécanique des Fluides de Toulouse (IMFT)—Allée Camille Soula, 31400 Toulouse, France
[2]CNRS, IMFT, 31400 Toulouse, France

(Received 25 March 2015; published 8 September 2015)

Gravity- or buoyancy-driven bodies moving in a slightly viscous fluid frequently follow fluttering or helical paths. Current models of such systems are largely empirical and fail to predict several of the key features of their evolution, especially close to the onset of path instability. Here, using a weakly nonlinear expansion of the full set of governing equations, we present a new generic reduced-order model based on a pair of amplitude equations with exact coefficients that drive the evolution of the first pair of unstable modes. We show that the predictions of this model for the style (e.g., fluttering or spiraling) and characteristics (e.g., frequency and maximum inclination angle) of path oscillations compare well with various recent data for both solid disks and air bubbles.

DOI: 10.1103/PhysRevLett.115.114501 PACS numbers: 47.55.D-, 45.40.-f, 47.20.Ky, 47.27.ed

Fluttering, tumbling, or spiraling trajectories are routinely observed with bodies falling or rising freely in a large expanse of fluid, such as autumn leaves or coins and millimeter bubbles released in water [1,2]. These familiar situations contain the essence of the behavior of engineering and living systems undergoing sideways drift because of some symmetry breaking related to the intrinsic couplings between the body and fluid, e.g., Ref. [3]. This is why noticeable and continuous efforts have been devoted over the last two decades to derive reduced-order models aimed at capturing the way these couplings govern the style of gravity- or buoyancy-driven motions of plates [4–8], disks [9], or bubbles [10] in a slightly viscous fluid.

All these models are grounded in a dynamical system expressing Newton's second law applied to the moving body and involving the hydrodynamic forces and torques it experiences. These loads are generally split into "inertia" effects related to the displaced fluid and "wake" effects resulting from the vorticity generated at the body surface, the two of them being assumed to superimpose linearly. Potential flow theory provides guidance to express the contribution of the former as a function of the instantaneous body acceleration, velocity, and rotation rate, while empirical expressions implicitly assuming a quasisteady behavior, i.e., no dependency on the wake past history, are used to obtain closed-form models for the latter as a function of the same variables, e.g., Refs. [7,8]. Obviously, the resulting models involve a set of prefactors that needs to be fitted on experimental or computational data. Besides the limitations inherent to the assumption of quasisteadiness in the case of rapid oscillations, these models suffer from two major weaknesses because they *postulate* but cannot *predict* two key characteristics of the system evolution, namely, the sub- or supercritical nature of the bifurcation that breaks the initial vertical path and the two- or three-dimensional nature of the subsequent path geometry. For instance, the primary transition experienced by millimeter rising bubbles was assumed to be subcritical in Ref. [10] but the combination of direct simulations [11] and global stability predictions [12] has now established that it is actually supercritical.

In this Letter we propose a new generic approach to this class of problems aimed at predicting the occurrence and characteristics of the first nonvertical regime. The resulting model overcomes the above limitations and does not require any empirical adjustment once the body characteristics are known. Besides shape and density, the latter include the nature of the surface, which allows the fluid to slip along the body in the case of bubbles and yields the usual no-slip condition for solid bodies. We derive this model by adopting a stability viewpoint and performing a rigorous weakly nonlinear expansion of the full set of governing equations, namely, the Navier-Stokes equations for the fluid, the Newton equations for the body, plus the boundary conditions that couple the two of them at the body surface. This yields a set of amplitude equations whose coefficients may be computed exactly for a given body. Considering contrasting situations, we demonstrate the capabilities of this model to predict the characteristics of the first nonvertical path that can be periodic, as in the zigzagging (or fluttering) and helical (or spiraling) regimes discussed below, or steady oblique as observed in some narrow range of parameters with spheres and light disks.

We consider thin cylinders (hereafter referred to as "disks") of thickness h, diameter d, and density ρ_b falling or rising freely under gravity or buoyancy in an unbounded fluid of kinematic viscosity ν_f and density ρ_f at rest at infinity. We also briefly consider oblate spheroidal bubbles with major and minor semiaxes b and a, respectively. In both cases the body is characterized by its volume $\mathcal{V}$, mass

M, and moment of inertia tensor $\mathbb{I}$. The problem involves three dimensionless control parameters. Effects of the body geometrical anisotropy are characterized by a geometrical aspect ratio, i.e., $\chi = d/h$ for disks and $\chi = b/a$ for spheroidal bubbles. Fluid and body inertia are compared through the body-to-fluid density ratio $\bar{\rho} = \rho_b/\rho_f$. Finally, buoyancy and viscous effects are compared through the Archimedes number $\mathrm{Ar} = U_g \ell_1/\nu_f$ involving the gravitational velocity $U_g = (|\bar{\rho} - 1| g \ell_2)^{1/2}$, with $\ell_1 = d$ and $\ell_2 = \frac{3}{16} h$ for disks, $\ell_1 = 2(ab^2)^{1/3}$ and $\ell_2 = \frac{1}{4}(ab^2)^{1/3}$ for spheroidal bubbles [13].

We formulate the problem in a system of axes (x, y, z) translating and rotating with the body, with the unit vector $\mathbf{e_x}$ collinear to the disk or bubble symmetry axis and directed upwards, and $\mathbf{e_y}$ and $\mathbf{e_z}$ lying in the body diametrical plane (see Fig. 1 in the Supplemental Material [14]). The body motion is described by the state vector $\mathbf{Q}^b = [\mathbf{U}(t), \mathbf{\Omega}(t), \mathbf{\Xi}(t)]^T$, where $\mathbf{U}$ and $\mathbf{\Omega}$ are the translational and rotational velocities, respectively, and $\mathbf{\Xi}$ is the angular position vector whose components are the roll, pitch, and yaw angles of the system, i.e., the angular positions of the x, y, and z axes with respect to fixed axes, respectively. For small angular deviations from vertical, the rotation rate is merely the time rate of change of $\mathbf{\Xi}$, i.e., $\mathbf{\Omega} = d_t \mathbf{\Xi}$. The fluid flow is described by the state vector $\mathbf{Q}^f = [\mathbf{V}(x, y, z, t), P(x, y, z, t)]^T$, where $\mathbf{V}$ is the local absolute velocity and P is the local pressure. The body path is governed by the rigid-body motion equations and the flow about it by the Navier-Stokes equations. The fluid-body couplings are provided by the fluid forces and torques on the one hand and the boundary conditions at the body surface $\mathcal{S}$ on the other hand. The full set of equations reads [15]

$$\boldsymbol{\nabla} \cdot \mathbf{V} = 0, \tag{1a}$$

$$\partial_t \mathbf{V} + (\mathbf{V} - \mathbf{W}) \cdot \boldsymbol{\nabla} \mathbf{V} + \mathbf{\Omega} \times \mathbf{V} = -\rho_f^{-1} \boldsymbol{\nabla} P + \nu_f \boldsymbol{\nabla}^2 \mathbf{V}, \tag{1b}$$

$$M(d_t \mathbf{U} + \mathbf{\Omega} \times \mathbf{U}) + (\rho_f \mathcal{V} - M)\mathbf{g} = \int_{\mathcal{S}} \mathbf{T} \cdot \mathbf{n} dS, \tag{1c}$$

$$\mathbb{I} \cdot d_t \mathbf{\Omega} + \mathbf{\Omega} \times (\mathbb{I} \cdot \mathbf{\Omega}) = \int_{\mathcal{S}} \mathbf{r} \times (\mathbf{T} \cdot \mathbf{n}) dS, \tag{1d}$$

$$d_t \mathbf{\Xi} = \mathbf{\Omega}, \tag{1e}$$

where $\mathbf{r}$ denotes the position vector relative to the body center of inertia, $\mathbf{W} = \mathbf{U} + \mathbf{\Omega} \times \mathbf{r}$ is the local entrainment velocity of the (x, y, z) axes, and $\mathbf{T} = -P\mathbf{I} + \rho_f \nu_f (\boldsymbol{\nabla} \mathbf{V} + {}^{\mathrm{T}}\boldsymbol{\nabla} \mathbf{V})$ is the stress tensor. The no-slip condition $\mathbf{V} = \mathbf{W}$ holds on the disk surface. In the case of a clean bubble, it is replaced by the zero penetration condition $\mathbf{V} \cdot \mathbf{n} = \mathbf{W} \cdot \mathbf{n}$ and the shear-free condition $\mathbf{n} \times (\mathbf{T} \cdot \mathbf{n}) = \mathbf{0}$, $\mathbf{n}$ denoting the local unit normal to $\mathcal{S}$. Finally, the fluid is at rest far from the body, implying $\mathbf{V} = \mathbf{0}$ for $\|\mathbf{r}\| \to \infty$.

The solution to Eq. (1) may be considered as a state vector $\mathbf{Q} = [\mathbf{Q}^f, \mathbf{Q}^b]^T$. For both types of bodies (and provided χ is large enough in the case of bubbles), a bifurcation to a nonvertical path occurs if the Archimedes number exceeds a threshold $\mathrm{Ar}_c(\chi, \bar{\rho})$ [11,12,15]. Thus we investigate the vicinity of this threshold by defining a small parameter $\epsilon = \sqrt{\mathrm{Ar} - \mathrm{Ar}_c}/\mathrm{Ar}_c$. To this aim, following Refs. [16,17], we introduce a two-time expansion procedure with a fast time scale t and a slow time scale $\tau = \epsilon^2 t$ so as to expand this solution in the form

$$\mathbf{Q} = \mathbf{Q}_0 + \epsilon \mathbf{q}_1(t, \tau) + \epsilon^2 \mathbf{q}_2(t, \tau) + \epsilon^3 \mathbf{q}_3(t, \tau) + \cdots. \tag{2}$$

The base state $\mathbf{Q}_0$ corresponds to the steady, vertical fall or rise with an axisymmetric flow field, and is computed as the solution of the nonlinear problem arising from the leading order of Eqs. (1a)–(1c). At order ϵ, $\mathbf{q}_1$ is the solution of the linear stability problem which is solved as in Refs. [15,18]. Taking advantage of the body axisymmetry, we express the fluid velocity and pressure fields in the body frame using cylindrical coordinates (x, r, φ) and seek this solution as a superposition of eigenmodes of the form $\hat{\mathbf{q}}_{\mathbf{1}m} = [\hat{\mathbf{q}}^f_m(x, r) e^{im\varphi}, \hat{\mathbf{q}}^b_m]^T e^{\lambda t}$, where m is the azimuthal wave number and $\lambda = \lambda_r + i\lambda_i$ is the complex eigenvalue. As shown in Refs. [15,18], the most unstable eigenmodes responsible for the bifurcation at $\mathrm{Ar} = \mathrm{Ar}_c$ always correspond to azimuthal wave numbers $m = \pm 1$.

The key result of this Letter is that these two modes also suffice to describe quantitatively the characteristics of the nonlinear fluttering and helical motions observed for $\mathrm{Ar} > \mathrm{Ar}_c$. Hence, restricting the following analysis to these modes, the general $O(\epsilon)$ solution may be expressed in the form $\epsilon \mathbf{q}_1 = \hat{A}^+(\tau)[\hat{\mathbf{q}}^f_{+1}(x, r) e^{+i\varphi}, \hat{\mathbf{q}}^b_{+1}]^T e^{i\lambda_{ic} t} + \hat{A}^-(\tau)[\hat{\mathbf{q}}^f_{-1}(x, r) e^{-i\varphi}, \hat{\mathbf{q}}^b_{-1}]^T e^{i\lambda_{ic} t} + \mathrm{c.c.}$, where $\hat{A}^{\pm}(\tau)$ are the $O(\epsilon)$ complex amplitudes of the two global modes, $\lambda_{ic} = \lambda_i(\mathrm{Ar}_c)$, and c.c. denotes the complex conjugate. We normalize these eigenmodes so that the norm of the corresponding angular position vector (i.e., the third component of $\hat{\mathbf{q}}^b_{\pm 1}$), say $\hat{\boldsymbol{\theta}}_{\pm 1}$, is unity. In this way, the maximum inclination of the body is merely $\theta_{\max} = |\hat{A}^+ + \hat{A}^-|$. Terms of order ϵ^2 and ϵ^3 in the expansion Eq. (2) are the solution of linear inhomogeneous problems arising from the Taylor expansion of Eq. (1) at the corresponding order. Details about the mathematical structure of these problems and the numerical procedure used to solve them with the FreeFem++ finite element software [19] are given in the Supplemental Material [14]. Note that in the simpler case where the axisymmetry of the base state is broken by a stationary bifurcation, a similar procedure allows realistic predictions of the occurrence and characteristics of the steady inclined paths that freely moving spheres, and sometimes disks, follow in some narrow range of Ar

[20]. Here, besides the growth rate, frequency, and spatial structure of the global mode $\mathbf{q_1}$, this procedure provides the pair of complex amplitude equations

$$d_t\hat{A}^{\pm} = (\mathrm{Ar} - \mathrm{Ar}_c)\sigma\hat{A}^{\pm} - \mu\hat{A}^{\pm}|\hat{A}^{\pm}|^2 - \nu\hat{A}^{\pm}|\hat{A}^{\mp}|^2, \quad (3)$$

where $(\mathrm{Ar} - \mathrm{Ar}_c)\sigma_r$ is the $O(\epsilon^2)$ exponential growth rate of $\mathbf{q_1}$ in the linear regime, $(\mathrm{Ar} - \mathrm{Ar}_c)\sigma_i$ is the $O(\epsilon^2)$ shift of the angular frequency resulting from the distance to the threshold (subscripts r and i denote the real and imaginary parts, respectively), and μ and ν are complex coefficients responsible for the nonlinear saturation. Coefficients σ, μ, and ν are computed so as to avoid resonant terms in the various linear problems encountered up to $O(\epsilon^3)$; details about the corresponding procedure based on the Fredholm alternative and the use of adjoint modes [21] are provided in the Supplemental Material [14] (see also Ref. [17]). The FreeFem++ scripts used to compute the above coefficients are available upon simple request [22].

The normal form (3) is characteristic of a Hopf bifurcation for a problem exhibiting an O(2) symmetry [23]. It is known to have two nontrivial solutions, namely, a rotating wave (RW) solution merely corresponding to one of the two possible helical modes $\hat{\mathbf{q}}_{\pm 1}$, and a standing wave (SW) solution made of the superimposition of two counterrotating modes $\hat{\mathbf{q}}_1$ and $\hat{\mathbf{q}}_{-1}$ with equal magnitudes. The RW (SW) solution is supercritical and stable only if $0 < \mu_r < \nu_r$ ($|\nu_r| < \mu_r$). In the context of buoyancy-driven bodies, the RW and SW paths correspond to a spiraling and a fluttering trajectory, respectively. The maximum inclination and frequency (or Strouhal number) of the body in the corresponding limit cycles respectively read $\theta_{\max}^{\mathrm{RW}} = |\hat{A}^{\pm}| = \sqrt{(\mathrm{Ar} - \mathrm{Ar}_c)\sigma_r/\mu_r}$ and $\mathrm{St}^{\mathrm{RW}} = (T/2\pi)[\lambda_{ic} + (\mathrm{Ar} - \mathrm{Ar}_c) \times \{\sigma_i - \sigma_r(\mu_i/\mu_r)\}]$ on the one hand, and $\theta_{\max}^{\mathrm{SW}} = |\hat{A}^{+} + \hat{A}^{-}| = 2\sqrt{(\mathrm{Ar} - \mathrm{Ar}_c)\sigma_r/(\mu_r + \nu_r)}$ and $\mathrm{St}^{\mathrm{SW}} = (T/2\pi)[\lambda_{ic} + (\mathrm{Ar} - \mathrm{Ar}_c)\{\sigma_i - \sigma_r[(\mu_i + \nu_i)/(\mu_r + \nu_r)]\}]$ on the other hand, the reference time scale being $T = \ell_1/U$ [24]. We computed the coefficients of Eq. (3) for bodies of various aspect ratios to examine how and up to which point this model predicts the occurrence and characteristics of fluttering and helical motions daily observed with falling or rising disks [25] and rising air bubbles [11].

We first consider a thick rising disk with $\chi = 3$ and $\bar{\rho} = 0.99$. Focusing on the inclination angle, the coefficients of the normal form (3) read $\sigma\mathrm{Ar}_c^2 = 69.73 + i39.85$, $\mu = 34.65 + i2.68$, and $\nu = 19.28 + i24.24$. Hence the model predicts that the SW path is the stable solution for $\mathrm{Ar} > \mathrm{Ar}_c$ (with $\mathrm{Ar}_c = 44.98$), in agreement with experiments [26] and DNS data [27] in which a fluttering path was detected for $\mathrm{Ar} \gtrsim 45$. Figure 1(a) provides evidence that the maximum disk inclination in that regime is also accurately predicted, even far from the threshold. In contrast, Fig. 1(b) reveals that the predicted frequency

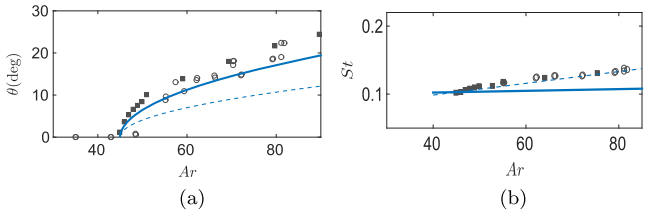

FIG. 1 (color online). Bifurcation diagram for a fluttering disk with $\chi = 3$ and $\bar{\rho} = 0.99$: (a) inclination angle; (b) frequency. The solid (dashed) line corresponds to the stable, i.e., SW (unstable, i.e., RW) branch. The open and closed symbols are data from experiments [26] and DNS [27], respectively.

agrees well with experimental and computational data only in the close vicinity of the threshold.

We now turn to the case of a thinner disk with $\chi = 6$ for which the vertical path becomes unstable at $\mathrm{Ar}_c = 41.81$. The corresponding coefficients of (3) read $\sigma\mathrm{Ar}_c^2 = 70.18 + i26.94$, $\mu = 34.65 - i26.21$ and $\nu = 44.17 + i22.23$. Hence the model now predicts a stable RW branch, in agreement with DNS and experiments which revealed a spiraling path beyond $\mathrm{Ar} \sim 43$ [26] (though these authors evidenced that the three-dimensional path gets more and more planar as Ar increases, eventually giving way to a purely planar zigzagging path for $\mathrm{Ar} \sim 55$). Figure 2(a) shows that the model accurately predicts the maximum disk inclination in the spiraling regime close to the threshold and becomes less reliable as the transition to flutter is approached. The frequency prediction [Fig. 2(b)] turns out to be more robust, its range of validity extending up to $\mathrm{Ar} \approx 70$. Note the clearly different slopes of the two curves St(Ar) corresponding to the RW and SW modes, respectively, which helps confirm that the first nonvertical path is of RW type. Next we turn to the case of a rising oblate bubble with an aspect ratio $\chi = 2.5$, a situation where the shear-free condition is substituted for the no-slip boundary condition at the body surface. In that case, global stability [12] indicates that the vertical path first becomes unstable at $\mathrm{Ar}_c = 32.14$ via a Hopf bifurcation, in agreement with DNS, where a transition to a planar zigzagging regime is detected at $\mathrm{Ar} \gtrsim 30$ [11]. The coefficients of the normal form (3) describing the inclination angle are

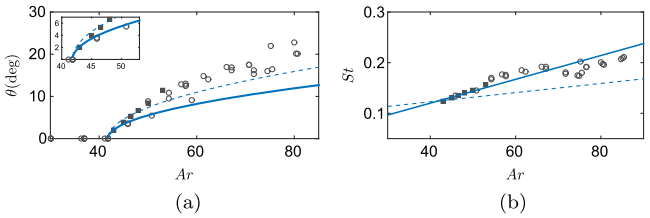

FIG. 2 (color online). Bifurcation diagram for a spiraling disk with $\chi = 6$ and $\bar{\rho} = 0.99$: (a) inclination angle; (b) frequency. Same convention as in Fig. 1, i.e., the solid (dashed) line now corresponds to the RW (SW) branch.

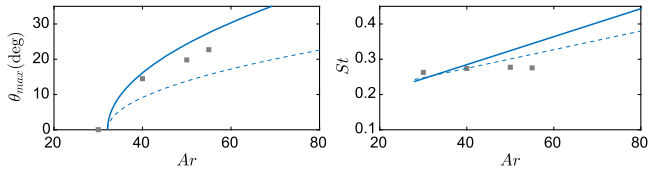

(a) (b)

FIG. 3 (color online). Bifurcation diagram for a fluttering oblate spheroidal bubble with $\chi = 2.5$ and $\bar{\rho} = 10^{-3}$: (a) inclination angle; (b) frequency. Same convention as in Fig. 1. The square symbols are DNS data from Ref. [11].

$\sigma \mathrm{Ar}_c^2 = 24.83 - i15.36$, $\mu = 7.42 - i9.71$, and $\nu = 2.14 - i6.10$. Therefore, the model correctly predicts that the SW mode is the stable solution selected by the bifurcation. Figure 3(a) shows that it also properly captures the sharp increase of the bubble inclination with the distance to the threshold up to $\mathrm{Ar} = 40$, although it tends to overpredict it at larger Ar. In contrast, according to Fig. 3(b), the model largely overestimates the weak increase of the frequency with $\mathrm{Ar} - \mathrm{Ar}_c$.

Last, we consider the case of an infinitely thin disk. In this situation, it is customary to define the relative disk inertia through the ratio $I^* = (\pi/64)\sigma_b/\rho d$, σ_b denoting the disk's surface density (the above two disks with $\chi = 3$ and $\chi = 6$ correspond to $I^* = 1.6 \times 10^{-2}$ and $I^* = 8.0 \times 10^{-3}$, respectively). Here we select a disk with a low relative inertia, $I^* = 4.0 \times 10^{-3}$, for which the linear stability analysis [15] reveals the existence of two distinct thresholds within a narrow range of Ar, yielding two distinct pairs of unstable modes. At the first of those thresholds ($\mathrm{Ar}_c^{\mathrm{sub}} = 35.8$), the corresponding coefficients of the normal form are found to be $\sigma \mathrm{Ar}_c^2 = 20.00 + i5.00$, $\mu = -5.82 - i8.62$, and $\nu = -0.34 - i6.28$. The negative signs of μ_r and ν_r imply that the corresponding bifurcation is subcritical. As shown by Fig. 4, it eventually leads to a large-amplitude fluttering regime whose characteristics and subcritical nature were described in Ref. [28], the corresponding DNS detecting its existence down to $\mathrm{Ar} \approx 33$.

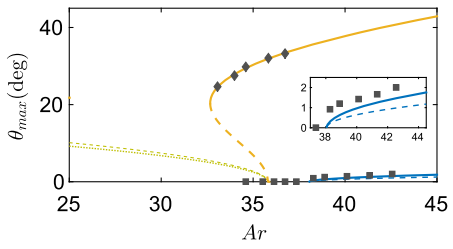

FIG. 4 (color online). Bifurcation diagram of the inclination angle of an infinitely thin disk with $I^* = 4 \times 10^{-3}$. Same convention as in Fig. 1 for the solid and dashed lines, the left (right) pair of which corresponds to the subcritical (supercritical) bifurcation. The two series of closed symbols are DNS data from Ref. [28]. The S-shaped curve is an empirical fit based on an extension of Eq. (3) up to terms of $O(\epsilon^5)$.

In contrast, the second bifurcation at $\mathrm{Ar}_c^{\mathrm{sup}} = 38.1$ is supercritical. It yields a second fluttering regime with tiny disk's oscillations. DNS [28] detected the existence of this second regime for $\mathrm{Ar} \geq 37.4$ and showed its frequency to be typically 3 times lower than that of the large-amplitude fluttering. As shown by Fig. 4, the model correctly reproduces the characteristics of this regime. It is, of course, unable to predict those of the large-amplitude fluttering, a task which would at least require its extension up to terms of $O(\epsilon^5)$ as shown by the fit displayed in Fig. 4. Previous works [20,28] have shown that subcriticality of the first bifurcation of thin disks depends much more on the aspect ratio than on the inertia ratio. This is why the thin disk with $\chi = 6$ and the infinity thin disk considered here behave so differently, despite the two close values of I^*. In the case of the bifurcation to the steady oblique regime [20], the threshold for the existence of a subcritical transition was found to be $\chi_c \approx 52$. However, there is no proof for the time being that this threshold is unchanged when the first nonvertical regime is unsteady.

In summary, we have derived a third-order truncated weakly nonlinear model aimed at predicting the characteristics of the path instability and first nonvertical regimes of buoyancy-driven axisymmetric bodies. Its strength originates from the absence of any tuning in the coefficients of the amplitude equations in which it is grounded, their value resulting from a mathematical compatibility condition. The examples reported in this Letter prove that this model faithfully predicts the supercritical or subcritical nature of the bifurcation and the type (fluttering vs spiraling) of path that follows. It also provides reliable predictions of the maximum body inclination and frequency of its oscillations in these regimes, irrespective of the boundary condition (no-slip vs shear-free) resulting from the nature of the body surface. Its range of validity extends from 30% up to 100% beyond the threshold $\mathrm{Ar} = \mathrm{Ar}_c$ and it might actually be further increased by selecting optimally the definition of the expansion parameter. From a generic viewpoint, the success of this approach proves that the first nonvertical path succeeding the initial straight vertical rise or fall merely results from the nonlinear saturation of the linear global modes of the coupled fluid-body system.

This approach can be used without any addition in many other situations of interest in fluid-structure interactions problems. For instance, the role of a passive appendage in the generation of a sideways drift was explored in Ref. [3] by considering a system made of a circular cylinder and a plate rigidly attached to it. The two-dimensional analog of our code can be employed to predict the results of the corresponding experiments and computations with fixed (but freely rotating) and buoyancy-driven systems, respectively. We are also currently working on the extension of this methodology to deformable bodies such as flags and drops which involve extra degrees of freedom associated with the time-dependent body geometry.

We acknowledge discussions with P. Ern and O. Marquet and thank F. Auguste for providing the DNS data used for comparison. This work was supported by the Agence Nationale de la Recherche under Grant No. ANR-09-BLAN-0132 OBLIC.

*Corresponding author.
magnau@imft.fr

[1] H. K. Moffatt, Three coins in a fountain, J. Fluid Mech. **720**, 1 (2013).
[2] P. Ern, F. Risso, D. Fabre, and J. Magnaudet, Wake-induced oscillatory paths of bodies freely rising or falling in fluids, Annu. Rev. Fluid Mech. **44**, 97 (2012).
[3] U. Lacis, N. Brosse, N. Ingremeau, A. Mazzino, F. Lundell, H. Kellay, and S. Bagheri, Passive appendages generate drift through symmetry breaking, Nat. Commun. **5**, 5310 (2014).
[4] Y. Tanabe and K. Kaneko, Behavior of a Falling Paper, Phys. Rev. Lett. **73**, 1372 (1994).
[5] L. Mahadevan, Tumbling of a falling card, C. R. Acad. Sci. Paris **323**, 729 (1996).
[6] A. Belmonte, H. Eisenberg, and E. Moses, From Flutter to Tumble: Inertial Drag and Froude Similarity in Falling Paper, Phys. Rev. Lett. **81**, 345 (1998).
[7] U. Pesavento and Z. J. Wang, Falling Paper: Navier-Stokes Solutions, Model of Fluid Forces, and Center of Mass Elevation, Phys. Rev. Lett. **93**, 144501 (2004).
[8] A. Andersen, U. Pesavento, and Z. J. Wang, Unsteady aerodynamics of fluttering and tumbling plates, J. Fluid Mech. **541**, 65 (2005).
[9] P. Ern, F. Risso, P. C. Fernandes, and J. Magnaudet, Dynamical Model for the Buoyancy-Driven Zigzag Motion of Oblate Bodies, Phys. Rev. Lett. **102**, 134505 (2009).
[10] W. L. Shew and J.-F. Pinton, Dynamical Model of Bubble Path Instability, Phys. Rev. Lett. **97**, 144508 (2006).
[11] G. Mougin and J. Magnaudet, Path Instability of a Rising Bubble, Phys. Rev. Lett. **88**, 014502 (2001).
[12] J. Tchoufag, J. Magnaudet, and D. Fabre, Linear instability of the path of a freely rising spheroidal bubble, J. Fluid Mech. **751**, R4 (2014).
[13] An alternative definition of the Archimedes number, say Ar_d, built on the equivalent diameter of the bubble, i.e., $\ell_1 = \ell_2 = 2(ab^2)^{1/3}$, has been used in previous works, e.g., Ref. [12], and is related to Ar through $\mathrm{Ar}_d = 2^{3/2}\mathrm{Ar}$.
[14] See Supplemental Material at http://link.aps.org/supplemental/10.1103/PhysRevLett.115.114501 for the perturbation procedure and the successive linear problems involved in the derivation of the normal form.
[15] J. Tchoufag, D. Fabre, and J. Magnaudet, Global linear stability analysis of the wake and path of buoyancy-driven disks and thin cylinders, J. Fluid Mech. **740**, 278 (2014).
[16] D. Sipp and A. Lebedev, Global stability of base and mean flows: A general approach and its applications to cylinder and open cavity flows, J. Fluid Mech. **593**, 333 (2007).
[17] P. Meliga, J.-M. Chomaz, and D. Sipp, Global mode interaction and pattern selection in the wake of a disk: A weakly nonlinear expansion, J. Fluid Mech. **633**, 159 (2009).
[18] J. Tchoufag, J. Magnaudet, and D. Fabre, Linear stability and sensitivity of the flow past a fixed oblate spheroidal bubble, Phys. Fluids **25**, 054108 (2013).
[19] F. Hecht, New development in FreeFem++, J. Numer. Math. **20**, 251 (2012).
[20] D. Fabre, J. Tchoufag, and J. Magnaudet, The steady oblique path of buoyancy-driven disks and spheres, J. Fluid Mech. **707**, 24 (2012).
[21] P. Luchini and A. Bottaro, Adjoint equations in stability analysis, Annu. Rev. Fluid Mech. **46**, 493 (2014).
[22] We encourage interested readers to contact us to apply our code to other problems. The CPU time required to obtain the coefficients of the normal form (3) is typically 1 h on an 8-core personal computer and the generation of the discretization grid requires less than 1 h.
[23] M. Golubitsky, I. Stewart, and D. Schaeffer, *Singularities and Groups in Bifurcation Theory* (Springer-Verlag, New York, 1988).
[24] We use $U = U_0$ (defined in the Supplemental Material [14]) for disks and $U = U_g$ for bubbles to ease the comparison with Ref. [11] [in that paper the reference length scale is $(ab^2)^{1/3}$ instead of $2(ab^2)^{1/3}$, so that the corresponding St have been multiplied by a factor of 2 in Fig. 3(b)].
[25] S. B. Field, M. Klaus, M. G. Moore, and F. Nori, Chaotic dynamics of falling disks, Nature (London) **388**, 252 (1997).
[26] P. C. Fernandes, F. Risso, P. Ern, and J. Magnaudet, Oscillatory motion and wake instability of freely rising axisymmetric bodies, J. Fluid Mech. **573**, 479 (2007).
[27] F. Auguste, Ph.D. thesis, Univ. Toulouse, France, 2010, http://thesesups.ups-tlse.fr/1186/.
[28] F. Auguste, J. Magnaudet, and D. Fabre, Falling styles of disks, J. Fluid Mech. **719**, 388 (2013).